CHEMICAL ENGINEERING TRANSACTIONS
VOL. 94, 2022
A publication of AIDIC
The Italian Association of Chemical Engineering
Online at www.cetjournal.it
Guest Editors: Petar S. Varbanov, Yee Van Fan, Jiří J. Klemeš, Sandro Nižetić

ISBN 978-88-95608-93-8; **ISSN** 2283-9216
DOI: 10.3303/CET2294230

Bleed-and-Refill Cycle Immersion-Based Corrosion Testing of SS304 and Al6061 Metals in E10 Ethanol-Gasoline Blends

Myron T. Alcanzare, Michael T. Castro, Joey D. Ocon*

Laboratory of Electrochemical Engineering (LEE), Department of Chemical Engineering, University of the Philippines Diliman, Quezon City 1101, Philippines
jdocon@up.edu.com

In this work, we propose an immersion corrosion measurement method with E10 bioethanol-gasoline blend on austenitic steel (SS304) and aluminum (Al6061). Immersion tests were designed to simulate a weekly refuel cycle and were performed over 4, 8, and 12-week durations. Polarization resistance, surface morphology, and corrosion products were then observed after the immersion tests. Corrosion rates were estimated from polarization resistance measurements *via* electrochemical impedance spectroscopy. Afterwards, the surface morphology of exposed samples was studied using scanning electron microscopy. Lastly, the corrosion products were characterized using scanning electron microscopy with energy dispersive X-ray analysis. Surface staining was observed in both metal substrates. It was observed that the corrosion rate of SS304 remained relatively constant throughout the immersion time. In contrast, an increment in the corrosion rate of Al6061 was observed after four weeks of immersion due to the peeling of the protective oxide layer.

1. Introduction

The large contribution of the transport sector to the emission of greenhouse gases has prompted governments to promote the use of biofuels for traditional vehicles (Solomon, 2010). In the Philippines, this is mandated by the Biofuels Act of 2007, which gradually increases the target amount of bioethanol to be blended with gasoline. The Philippine government aimed to have ethanol-gasoline blends (EB) containing 20% ethanol by volume (E20) by 2020, but commercially available blends have been limited to E10 due to the low production of bioethanol relative to the demand of fuel (Bedford and Corpuz, 2021)

Despite the advantages of bioethanol, it has properties that increase the likelihood of corrosion. For example, bioethanol samples have been found to contain contaminants (Baena et al., 2012) that are present in either the feedstock or the pre-treatment processes (Lamounier et al. 2020). The hygroscopic property of bioethanol is also observable even when blended as EB. The absorption of water into EB may result in the formation of water pockets via phase separation (Christensen et al., 2021). Ionic contaminants would migrate into the aqueous layer and have a higher localized concentration than that of the bulk. This improves the conductivity of the EB which makes it behave like an electrolyte for a corrosion cell (Jafari et al., 2011).

This has motivated several studies on the corrosive properties of EB. Many of these studies investigated the effects of contaminant concentration (Abel and Virtanen, 2015) and corrosion resistance (Ambrozin et al., 2010) of different metals using standardized testing methods such as ASTM G31 and SAE J1747 (Bones et al., 2009). To the best of our knowledge, only Mould (2009) utilized a test setup wherein the container itself is the corrosion substrate. The methodology employs a cyclic filling immersion test that simulates the conditions in a gasoline tank by periodically replacing the contents of the container. This replenished the supply of contaminant ions while accumulating the corrosion products on the surface of the samples. However, they did not characterize the immersed samples. In contrast, Jafari et al. (2011) characterized the metal substrates to estimate the corrosion rates. Impedance data collected from electrochemical impedance spectroscopy (EIS) were used to determine the resistances and capacitances in an equivalent circuit, from which the annual corrosion rate can be determined without performing a mass loss experiment.

In this work, a proof-of-concept immersion method was used to analyze the corrosive properties of E10 blends in fuel tanks made from austenitic steel (SS304) and aluminum (Al6061). These metals were selected as they

Paper Received: 27 April 2022; Revised: 10 May 2022; Accepted: 5 June 2022
Please cite this article as: Alcanzare M.T., Castro M.T., Ocon J.D., 2022, Bleed-and-refill Cycle Immersion-based Corrosion Testing of Ss304 and Al6061 Metals in E10 Ethanol-gasoline Blends, Chemical Engineering Transactions, 94, 1381-1386 DOI:10.3303/CET2294230

are often used in the construction of automotive fuel tanks. The metal substrates were characterized via EIS to estimate the corrosion rate of the metal substrates and subjected to scanning electron microscopy with energy dispersive X-ray spectroscopy (SEM-EDX), tests to obtain images of surface morphology and presence of key elements that are associated with the metals and E10 blends.

2. Methodology

2.1 Materials

The E10 blend used in this study is Fuel Save™ Gasoline from Shell™ Philippines. This product has a research octane number of 93 and contains additives in the form of lubricants and detergents. According to the specification sheet provided by the manufacturer, it is mainly composed of cracked naphtha, 2-ethoxy-2-methylpropane, 2-methoxy-2-methylpropane, 2-methoxy-2-methylbutane, and ethanol. The fuel was purchased weekly along Marcos Highway, Antipolo City, Philippines and was used in the same day. It was stored in an E10 compatible high-density polyethylene (HDPE) gasoline container that was washed with detergent, rinsed with distilled water, and dried on a weekly basis prior to use. EIS tests were done using a three-electrode setup. The working electrodes (WE) were the metal substrates prepared from immersion testing. The counter electrode (CE) was a 0.5 mm platinum wire that was cleaned with Piranha etch solution prior to use. The reference electrode (RE) was a Metrohm double junction Ag/AgCl 6.0726.100 electrode filled with 3.0 M KCl.

2.2 Cyclic filling immersion test

Corrosion cups made from SS304 and Al6061 were fabricated with an inner diameter of 40 mm and a depth of 30 mm. The cups were dry polished using rotary tool-mounted silicon-carbide (SiC) paper with grit numbers 60, 120, 240, 480, and 600 in increasing grit numbers. The corrosion cups were then filled with acetone and ultrasonicated for 10 minutes to remove contaminants from the fabrication. Afterwards, the corrosion cups were rinsed with deionized water, dried with compressed dry air (CDA), and stored in a dry box prior to use.

In the cyclic filling immersion test, the corrosion cups were filled with 20 mL of E10 blend and sealed airtight to minimize water intake from the atmosphere. The samples were prepared in triplicate for each type of metal tested. Each cup was then stored in a 30.5 cm × 12.5 cm × 15.3 cm (L × H × W) HDPE container filled with sodium bentonite clay preheated to 35 °C. This container was then placed in a Cole Parmer incubator at 38 °C. The E10 blend was replenished every seven days by drawing 10 mL of fuel from each cup and replacing it with an equal volume of freshly procured E10 blend. The immersion test lasted 84 days and provided results for 4, 8, and 12 weeks of cyclic immersion.

To prepare the samples for analysis in SEM, the corrosion cups were drained and then dried with CDA. Afterwards these samples were cut using a handsaw to a height of 20 mm. A manual cutting method was selected to prevent heating the sample beyond 100 °C and to avoid the use of cutting fluids. Loose particles from sawing were then removed with CDA. Afterwards, these samples were placed in a dry box. Preparations for EIS and SEM-EDX were performed by taking 3 cm × 3 cm samples from the corrosion cups using a handsaw. The edges were then smoothened with 60-grit SiC paper to provide sufficient contact between the sample and the rubber seal of the corrosion cell in the EIS test. Metal substrate samples were taken every 28 days and prepared for the analysis tests.

2.3 Electrochemical analysis

EIS was selected as the electrochemical characterization technique due to the low conductivity of E10 blends. Figure 1 illustrates the three-electrode setup used in EIS. The plastic frame of the corrosion cell was made from polytetrafluoroethylene (PTFE). The WE was placed on the copper disk that served as the bottom contact that will be connected to the WE and sensing ports of the potentiostat. The contact between the corrosion cell and the copper disk was tightened to prevent leakage of E10. A gap space of 1 mm between the WE and CE was maintained as recommended by Baena et al. (2012). A 3D-printed polylactic acid (PLA) plastic RE holder was used to maintain a constant distance between the RE and CE. The corrosion cell was then filled with E10 until the RE was submerged by at least 3 cm. Unlike the cyclic immersion tests, the E10 blend in the corrosion cell was not refreshed during EIS. The lid was then closed to minimize exposure of the liquid to the atmosphere.

EIS was performed with a PGSTAT-302N potentiostat from MetroOhm Autolab, while fitting of EIS data to the equivalent circuit was performed using the NOVA 2.0 sofware. A 10-minute stabilization period was provided prior to EIS runs. The potentiostat was operated with an uninterruptible power supply and the setup was placed inside a grounded Faraday cage. EIS was conducted at room temperature with an amplitude of 50 mV rms. The observed frequency range was from 100 kHz to 100 mHz.

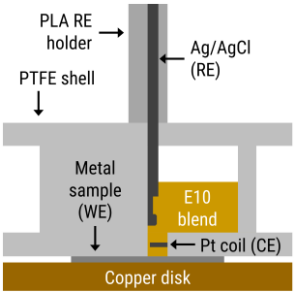

Figure 1: Illustration of the three-electrode setup used in EIS.

The corrosion rate is usually calculated using Tafel plots to obtain the overpotential and corrosion current. However, this cannot be done with E10 blends due to their low electrical conductivity. Jafari and co-workers estimated the corrosion current based on the equivalent circuit shown in Figure 2. In this circuit, R_s is the resistance due to conductivity of the EB, R_p is the polarization resistance that limits charge transport between the metal substrate and the EB, and C is the capacitance caused by build-up of corrosion products on the metal substrate. The corrosion current is computed based on the polarization resistance as shown by Equation 1. This equation was developed by Jafari et al. (2011) for samples exposed to E5 or E10 blends. In this equation, i_{corr} [mA cm^{-2}] is the corrosion current density and R_{p} [Ω cm^2] is the polarization resistance obtained from EIS tests.

$$i_{\mathrm{corr}} = \frac{1}{46R_{\mathrm{p}}} \tag{1}$$

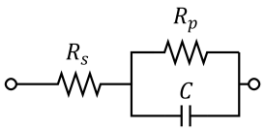

Figure 2: Equivalent circuit from which the corrosion current is estimated.

Equation 2 estimates the corrosion rate (CR) in milli-inches per year (mpy) based on the number of electrons flowing per unit area of metal and the thickness of a metal atom layer. The values of density ρ [g cm^{-3}], valence number of the metal n, and molecular weight M [g mol^{-1}] suggested by Jafari et al. (2011) for the metals considered are 7.8 g cm^{-3}, 2, and 56 g mol^{-1} for SS304, and 2.7 g cm^{-3}, 3, and 27 g mol^{-1} for Al6061. The corrosion rate estimated from the samples was integrated to determine the total thickness corroded.

$$\mathrm{CR} = \frac{129 i_{\mathrm{corr}} M}{n\rho} \tag{2}$$

The surfaces of the samples immersed for 4, 8, and 12 weeks were qualitatively monitored via SEM, and the elements present on the surfaces immersed after 12 weeks were also analyzed using EDX.

3. Results and discussion

3.1 Corrosion rate

The Nyquist plots generated from EIS measurements of the samples with different durations of immersion are shown in Figure 3a and 3b. The corresponding fitting parameters are shown in Table 1. The immersed Al6061 samples show a drop in polarization resistance compared to the control sample, which suggests the removal of passivation like an oxide layer. In contrast, the immersed SS304 samples have similar impedances with the control sample, which implies that long term immersion does not produce significant changes. Figure 3c compares the corrosion rates of the metal samples at various immersion lengths. As mentioned earlier, the corrosion rate of Al6061 increases greatly after long term immersion. The corrosion rate of SS304, however, increases by a much smaller amount after immersion.

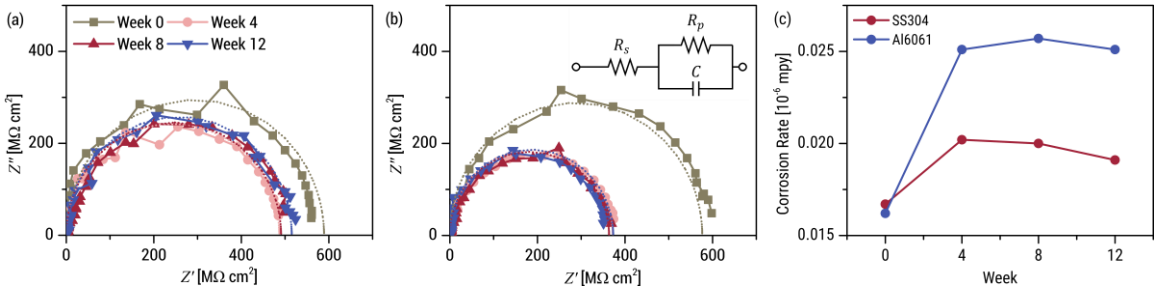

Figure 3: Nyquist plots generated from immersed SS304 (a) and Al6061 (b) samples, and the corrosion rate estimated from the polarization resistance (c). The radius of the semicircle in the Nyquist plots increases with the polarization resistance.

Table 1: Fitting parameters from the EIS measurements

Time	SS304 R_s [kΩ cm^2]	SS304 R_p [kΩ cm^2]	SS304 C [pF cm^2]	Al6061 R_s [kΩ cm^2]	Al6061 R_p [kΩ cm^2]	Al6061 C [pF cm^2]
Week 0	-4.79	589.05	111.53	-4.90	576.48	113.88
Week 4	-3.94	486.95	142.16	-4.37	372.28	166.50
Week 8	-4.85	490.87	124.88	-4.56	363.64	135.87
Week 12	-5.06	515.22	108.38	-4.01	373.06	159.44

3.2 Surface morphology

The SEM images of the immersed SS304 samples are presented in Figure 4a. There was no observed signature of pitting or formation of general corrosion on the surfaces. This is consistent with the findings of Baena and co-workers that SS304 is corrosion resistant and compatible with ethanol blends as it produces a protective chromium oxide passivation layer (Baena et al., 2012). Items pointed by the arrows appear to be organic foreign material. These have likely been deposited from the E10 blend because the samples were not rinsed with acetone after the immersion test. A site with foreign organic material, as shown in Figure 4b, was selected for elemental analysis to estimate its carbon content. The EDX spectrum is presented in Figure 4c. The large amount of C suggests that the foreign material is mainly composed of long-chain hydrocarbons and is an organic residue.

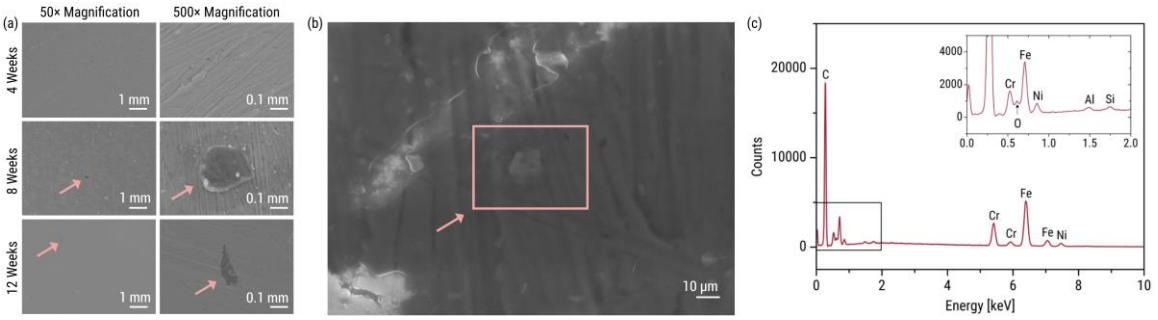

Figure 4: SEM images of the immersed SS304 samples (a), closeup of organic residue found on the sample (b), and EDX spectrum of the organic residue (c).

The SEM images of the immersed Al6061 samples are presented in Figure 5a. The oxide layer appears to slowly peel away with extended immersion periods until only a small amount of the oxide layer remains. The surface gradually smoothens and transitions into a less reflective film in 12 weeks, which is evident at a low magnification. This similar to the results observed by Thomson et al. (2013) in aluminum substrates exposed to dehydrated ethanol. In their study, the authors concluded that the oxide layer cracks and is eventually removed as it is attacked and replaced by an alcohol-based corrosion product that is slightly soluble in ethanol. Elemental analysis was performed on the site with the oxide layer peel-off signature shown in Figure 5b. The EDX spectrum is presented in Figure 5c. Small amounts of Mg and Ca were observed, which may have been ionic contaminants

from the feedstock used in producing the E10 blend. High amounts of C in the cavity suggests organic residue on the Al6061 samples that are similar to that observed on SS304 samples.

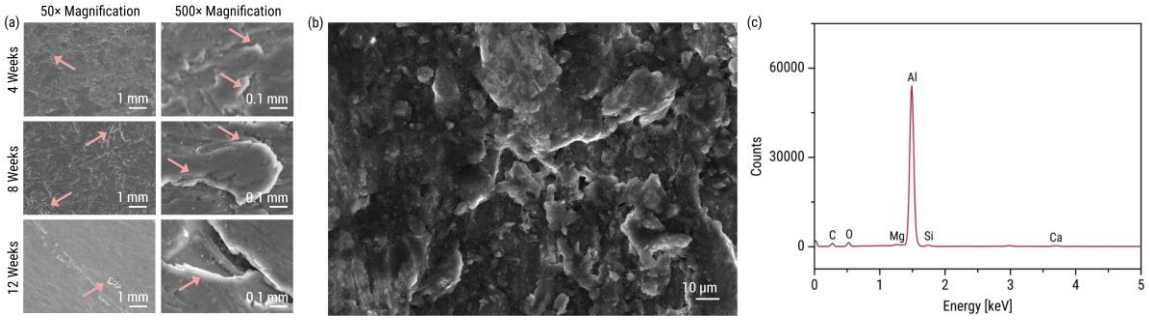

Figure 5: SEM images of the immersed Al6061 samples (a), closeup of oxide layer peeling found on the sample (b), and EDX spectrum of the exposed aluminium (c).

3.3 Discussion

In both metals, there are spots with high amounts of carbon in the sample. A possible explanation for the stains on the surface of the metal could be gum residue as these are heavier and less volatile than the components of gasoline. In a review article written by Pradelle et al. (2015), they repeated a claim that FCC-reformed naphtha have olefins that are more favorable to gumming as compared to those that had naphtha cracked via thermal cracking. Formation of this residue could be favored due to use of gasoline that had been blended with cracked naphtha using fluidized catalytic cracking (FCC).

The Al6061 samples experienced a large increase in corrosion rate after four weeks of immersion testing. This can be explained by the study of Sharipov and Starik (2015), which demonstrated that the rate constant of the reaction between aluminum and ethanol is much higher than that of aluminum oxide and ethanol. The reaction of the ethanol with aluminum became much faster upon removal of the oxide layer, which explains the increased corrosion rate of immersed samples.

Ethanol seeps into crevices wherein the passivation layer is damaged. The ethanol then attacks the aluminum and forms an alkoxide that strains the passivation layer due to volume expansion. The alkoxide is soluble in the alcohol, and it leaves the passivation layer open to reaction with ethanol. This results in the peel-off signature in the SEM images. More of the layer is peeled off over time and more of the unprotected aluminum is exposed. To the best of our knowledge, an analogous mechanism has not yet been reported for SS304.

This proposed mechanism, however, does not directly translate to higher rates of corrosion. In fact, the change in corrosion rate after the fourth week is less than 5%, which is within the margin of error. The area of aluminum that is open to attack after four weeks is therefore comparable to that at 12 weeks, and the only difference is the amount of oxide layer removed. This suggests that the gap between the oxide layer and the metal surface has sufficiently expanded after four weeks, and the corrosion rate of 2.51×10^{-8} mpy remains constant at longer immersion times. This is supported by the SEM images, which suggest that the bottom layer is already exposed by the fourth week.

The estimated corrosion rate in Al6061 in this study is different from those with setups at higher temperatures or higher concentrations of water. Thomson et al. (2013) showed that alcohol attacks aluminum with rapid corrosion at temperatures above 80 °C. Krüger et al. (2012) demonstrated that corrosion becomes significant at 60 °C and less than 0.2% water by volume. However, these studies also observed the dry corrosion of aluminum in alcohol, which is consistent with the proposed corrosion mechanism in this study. The accumulated water content using the cyclic filling immersion method therefore did not reach the threshold for favoring aluminum oxide formation.

4. Conclusions

In this work, we presented a cyclic filling immersion test to estimate the corrosion rates of metals upon exposure to EB under operating conditions identical those of fuel tanks for internal combustion engine vehicles. SS304 and Al6061 samples were subjected to the immersion test, and the surface morphology and corrosion products were determined after varying immersion durations. SS304 samples did not show noticeable signs of pitting or general corrosion. In contrast, Al6061 samples were seen to have an oxide layer that was slowly removed during prolonged exposure. Al6061 showed a trend of increasing corrosion rate after being immersed, which was not observed in SS304. Gum residue, a known product of olefin oxidation with dissolved oxygen in the gasoline,

was suspected in all the samples. The presence of such is therefore not reliant on the type of metal used as container.

The following improvements for further research that were not included in the scope of this study are recommended.

1. Use of 1.0 M LiCl in ethanol solution instead of KCl and fabrication of a corrosion cell with embedded Pt gauze for better stability in EIS. Lou and Singh (2010) explained that LiCl is soluble in ethanol and causes the electrolyte to better disperse in the sample. This property could allow for lower amplitudes and frequencies that were unattainable in this study due to instability of EIS.
2. A statistical analysis on the effects of other factors (e.g., material composition, EB composition, temperature, cycle length, dissolved oxygen, moisture, etc.) on the corrosion rate.
3. Quantitative determination of the metal samples' composition via X-ray photoemission spectroscopy.
4. Complete chemical analysis of the gasoline sample via gas chromatography at the end of the cyclic immersion test to determine if there is an increase in the number of contaminants.
5. A comparative study of the cyclic filling immersion test and existing standard methods.
6. A comparison of polarization resistances observed from different equivalent circuits, and how the polarization resistance relates to the surface morphology.

Acknowledgments

M.T.A. would like to acknowledge Don Felipe Say and Theresa Chua Say Professorial Chair Award and the Department of Science and Technology Engineering Research and Development for Technology (DOST-ERDT) program. This research is funded through the Enhanced Creative Work and Research Grant (ECWRG) of the University of the Philippines Office of the Vice President for Academic Affairs (UP OVPAA).

References

Solomon B. D., 2010, Biofuels and sustainability, Annals of the New York Academy of Sciences, 1185, 119–134.

Bedford R., Corpuz P., 2020, Biofuels annual, US Department of Agriculture Foreign Agricultural Service <https://apps.fas.usda.gov/newgainapi/api/Report/DownloadReportByFileName?fileName=Biofuels%20Annual_Manila_Philippines_10-26-2020> accessed 29.12.2021

Baena L.M., Gómez M., Calderón J.A., 2012, Aggressiveness of a 20% bioethanol-80% gasoline mixture on autoparts: I behavior of metallic materials and evaluation of their electrochemical properties, Fuel, 95, 320–328

Lamounier K.F., Rodrigues P.O., Pasquini D., Santos A.S., Baffi M.A., 2020, Effects of the increase in substrate load and hydrolysis time in the saccharification of sugarcane bagasse and ethanol production, Holos, 6

Christensen E.D., McCormick R.L., Water uptake and weathering of ethanol-gasoline blends in humid environments for the renewable fuels association, National Renewable Energy Laboratory <https://www.hondatwins.net/attachments/evaluation-of-water-uptake-by-ethanol-rfa-09-16-pdf.301951/> accessed 29.12.2021

Jafari H., Idris M.H., Ourdjini A., Rahimi H., Ghobadian B., 2011, EIS study of corrosion behavior of metallic materials in ethanol blended gasoline containing water as a contaminant, Fuel, 90, 1181–1187

Mould P.R., 2009, Corrosion resistance of various steel fuel tank systems in alcohol-containing fuels, Automotive Fuels Conference 2009, Dearborn, MI

Ambrozin A.R.P., Monteiro M.R., Santos A.O., 2010, Kuri S.E., Evaluation of galvanic corrosion of a Zn alloy in alcohol fuel, Fuel Processing Technology, 91, 1687–1690

Abel J., Virtanen S., 2015, Corrosion of martensitic stainless steel in ethanol-containing gasoline: Influence of contamination by chloride, H2O and acetic acid, Corrosion Science, 98, 318–326

Thomson J.K., Pawel S.J., Wilson D.F., 2013, Susceptibility of aluminum alloys to corrosion in simulated fuel blends con-taining ethanol, Fuel, 111, 592–597

Sharipov A.S., Starik A.M., 2015, Theoretical study of the reactions of ethanol with aluminum and aluminum oxide, Journal of Physical Chemistry A, 119, 3897–3904

Krüger L., Tuchscheerer F., 2012, Mandel M., Müller S., Liebsch S., Corrosion behaviour of aluminium alloys in ethanol fuels, Journal of Materials Science, 47, 2798–2806

Lou X., Singh P.M., 2010, Role of water, acetic acid and chloride on corrosion and pitting behaviour of carbon steel in fuel-grade ethanol, Corrosion Science, 52, 2303–2315

Pradelle F., Braga S.L., Martins A.R.F.A., Turkovics F., and Pradelle R.N.C., 2015, Gum formation in gasoline and its blends: a review, Energy and Fuels, 29, 7753–7770